



Reactive transport impacts on recovered freshwater quality during multiple partially penetrating wells (MPPW-)ASR in a brackish heterogeneous aquifer



Koen G. Zuurbier^{a, b, *}, Niels Hartog^{a, c}, Pieter J. Stuyfzand^{a, b}

^a KWR Watercycle Research Institute, P.O. Box 1072, 3430 BB, Nieuwegein, The Netherlands

^b Technical University Delft, Faculty of Civil Engineering, P.O. Box 5048, 2600 GA, Delft, The Netherlands

^c Utrecht University, Faculty of Geosciences, P.O. Box 80021, 3508 TA, Utrecht, The Netherlands

ARTICLE INFO

Article history:

Received 16 May 2015

Received in revised form

23 May 2016

Accepted 24 May 2016

Available online 26 May 2016

Keywords:

Aquifer storage and recovery

ASR

Multiple partially penetrating wells

MPPW

Reactive transport

Water quality

Cation exchange

Arsenic

Subsurface iron removal

Coastal aquifers

ABSTRACT

The use of multiple partially penetrating wells (MPPW) during aquifer storage and recovery (ASR) in brackish aquifers can significantly improve the recovery efficiency (RE) of unmixed injected water. The water quality changes by reactive transport processes in a field MPPW-ASR system and their impact on RE were analyzed. The oxic freshwater injected in the deepest of four wells was continuously enriched with sodium (Na^+) and other dominant cations from the brackish groundwater due to cation exchange by repeating cycles of 'freshening'. During recovery periods, the breakthrough of Na^+ was retarded in the deeper and central parts of the aquifer by 'salinization'. Cation exchange can therefore either increase or decrease the RE of MPPW-ASR compared to the RE based on conservative Cl^- , depending on the maximum limits set for Na^+ , the aquifer's cation exchange capacity, and the native groundwater and injected water composition. Dissolution of Fe and Mn-containing carbonates was stimulated by acidifying oxidation reactions, involving adsorbed Fe^{2+} and Mn^{2+} and pyrite in the pyrite-rich deeper aquifer sections. Fe^{2+} and Mn^{2+} remained mobile in anoxic water upon approaching the recovery proximal zone, where Fe^{2+} precipitated via MnO_2 reduction, resulting in a dominating Mn^{2+} contamination. Recovery of Mn^{2+} and Fe^{2+} was counteracted by frequent injections of oxygen-rich water via the recovering well to form Fe and Mn-precipitates and increase sorption. The MPPW-ASR strategy exposes a much larger part of the injected water to the deeper geochemical units first, which may therefore control the mobilization of undesired elements during MPPW-ASR, rather than the average geochemical composition of the target aquifer.

© 2016 Elsevier Ltd. All rights reserved.

1. Introduction

Aquifer storage and recovery (ASR) using wells can be a successful freshwater management tool in coastal areas worldwide by keeping temporary freshwater surpluses available for periods of shortage (Pyne, 2005). Freshwater surpluses are stored this way for later use in times of demand, creating a self-sufficient freshwater supply which makes external freshwater supply (including infrastructure) and/or costly desalination superfluous. However, application of especially small-scale ASR systems in aquifers with brackish or saline groundwater often results in a low recovery efficiency (RE: part of the injected water that can be recovered with a satisfying quality) due to buoyancy effects (Ward et al., 2009;

Zuurbier et al., 2013). Also, the buoyancy effects may preclude a progressively improving water quality with subsequent cycles as observed at conventional ASR systems (Ward et al., 2009). Recently, the use of multiple partially penetrating wells (MPPW) installed in a single borehole in a brackish aquifer allowed significantly higher recovery efficiencies by deep injection and shallow recovery, as demonstrated for relatively unmixed rainwater containing $<0.5 \text{ mmol/l Na}^+$ (Zuurbier et al., 2014). While that study focused on the buoyancy and mixing effects on the conservative transport of chloride (Cl^-), other water quality parameters may determine the final success of ASR, depending on the intended use. Sodium (Na^+), for example, may threaten the water quality for irrigation since it is toxic in low concentrations for various plants or crops (Kronzucker and Britto, 2011), but also for drinking and industrial purposes. Also, arsenic is known to be toxic for both humans and plants (National Research Council, 1977). Besides toxic effects, operational aspects, such as the clogging of pumps, pipelines, and

* Corresponding author. KWR Watercycle Research Institute, P.O. Box 1072, 3430 BB, Nieuwegein, The Netherlands.

E-mail address: koen.zuurbier@kwrwater.nl (K.G. Zuurbier).

sprinklers by the precipitation of manganese or iron oxides, may determine the suitability of the recovered water for direct use (Pyne, 2005). Especially for agricultural end users, recovered water upon aquifer storage ought to be directly usable to limit the water costs. Although the elements of concern are typically low in ASR 'injection water' (i.e. the water that is to be injected, after which it becomes 'injected water'), enrichment may occur by freshening and salinization (e.g., Appelo, 1994a, 1994b; Stuyfzand, 1993; Valocchi et al., 1981) and dissolution of carbonates (Antoniu et al., 2012; Stuyfzand, 1998). Additionally, the injection of oxygen and/or nitrate-containing water in a deeply anoxic target aquifer may induce mobilization of SO_4 , Fe, Mn, and As, which has been reported in ASR studies worldwide (e.g., Antoniou et al., 2012; Jones and Pichler, 2007; Neil et al., 2014; Price and Pichler, 2006; Stuyfzand, 1998; Vanderzalm et al., 2011; Wallis et al., 2010, 2011).

The operation of an MPPW-ASR system does not comply with the more traditional ASR-theories for bi-directional horizontal flow directions during injection and recovery via fully penetrating well screens in aquifers without significant buoyancy effects. During MPPW-ASR, instead, (oxygen-rich) freshwater is predominantly injected in brackish aquifers via the deeper wells while extraction occurs at shallower wells. Consequently, vertical transport exposes the injected water to a vertical range of geochemical heterogeneities in the aquifer and the associated potential sources of water quality deterioration. Additionally, hydrochemical conditions at the deeper wells are highly dynamic, with frequent alternations of freshening (during injection) and salinization (during storage/recovery). In this study, therefore, we analyzed the observed water quality changes by reactive transport processes in a field MPPW-ASR system with a focus on cation-exchange and redox-reactions and their impact on the RE. Hydrochemical data were collected during the field MPPW-ASR pilot in a brackish aquifer for which Zuurbier et al. (2014) described the hydrological aspects and freshwater recoverability based on *conservative transport* (chloride). The aim of this study was to assess for the same MPPW-ASR system how *reactive transport* processes affected the concentrations of Na^+ , Fe^{2+} , Mn^{2+} , and As in the recovered water over time. This provides a more complete analysis of the application and operational optimization of MPPW-ASR systems.

2. Materials and methods

The application of an MPPW-ASR system in a brackish aquifer was well-monitored in a field pilot in 2012 and 2013 allowing to closely analyze the water quality development in the aquifer until recovery. This field pilot was preceded by a detailed physical and geochemical characterization of the aquifer to understand the flow patterns and water quality changes.

2.1. ASR field site

The Nootdorp MPPW-ASR system was built in 2011 with the aim to store rainwater collected by the roof of a 20,000 m² greenhouse, and to recover this water for irrigation purposes in the same greenhouse (more details in Zuurbier et al., 2014). The MPPW, with four independently operated well screens at distinct aquifer intervals installed in a single borehole, were used to maximize the freshwater recovery (Fig. 1). The ASR system was extensively monitored for this study from January 2012 until September 2013.

The unconsolidated target aquifer is confined by unconsolidated clay and peat. Geological characterization indicated that the target aquifer consists of middle-coarse to very coarse fluvial sands from the Rhine River (Zuurbier et al., 2014). The lower part (HU-f-i, Fig. 3) is a little coarser than the upper part (HU-a-c). A fine sand layer (HU-d) and a sand layer containing reworked clay and peat deposits

in a coarse sand matrix (HU-e) are present in the middle of the target aquifer. This HU-e unit is discontinuous and found only locally in the pilot area (Zuurbier et al., 2014). Besides local separation into two compartments by the clayey interval of this HU-e unit, the aquifer is relatively homogeneous, as indicated by geophysical and hydrochemical analysis during the first ASR cycle (Zuurbier et al., 2014).

2.2. Operation of the MPPW during the Nootdorp ASR pilot

The injection rate was equally distributed over all MPPW screens in the first 3 months (Fig. 2). From April 2012 until May 2013 only the lower three well screens (AWS2–4) were used for injection, while mainly the shallow AWS1 and AWS2 were used for recovery, accompanied by a low-rate recovery at AWS3 in Cycle 2. The freshwater surpluses in the last phase (Summer, 2013) were injected at AWS1–4 from May 2013 until August and at AWS1–S3 during the last month of the pilot. During the pilot phase, 39.9% (11,591 m³) of the injected water (29,047 m³) was abstracted.

2.3. Site characterization and hydrochemical monitoring

2.3.1. Physical and geochemical sediment analyses

To characterize the target aquifer and identify potentially reactive intervals 114 samples were taken from thin-wall tubes at intervals of 0.2 m or smaller whenever lithological variations appeared (Zuurbier et al., 2014), or from the bailer at the other intervals of MW1 (every meter, n = 14). Grain size distribution of each sample was determined using a laser particle sizer (Zuurbier et al., 2014). Hydrogeological units (HU-a to HU-h) and their hydraulic properties were derived using the grain size distributions, head responses at MW1 upon pumping, and the breakthrough curves of Cl^- at MW1 (Zuurbier et al., 2014). Sedimentary organic matter (SOM) and total carbonates were deduced from thermogravimetry (TGA at 330, 550, 1000 °C).

An XRF-core scan (Avaatech, The Netherlands) was executed on the cut cores for a semi-quantitative analysis of Al, S, Ca, Mn, and Fe on a split-core-surface area of 1 cm² over a time interval of 10 s using a generator setting of 10 kV. This way, reliable log-ratios of Fe/S, Fe/Ca, Mn/Ca, and S/Ca were obtained, which are linearly related to the log-ratios of quantitative element concentrations (Weltje and Tjallingii, 2008). Sediments samples were taken at 6 distinct depth intervals and sent for laboratory XRF to correct the log-ratios obtained by the high-resolution core-scan. The reader is referred to the [Supplementary Information](#) for more details on the log-ratio correlation derived. True elemental ratios were subsequently attained via these log-ratios and corrected for molar masses. S/Ca was used to derive the part of Fe/Ca that is related to pyrite, assuming $\text{Fe} = 0.5 \times \text{S}$. This way the potential relative presence of Ca, Fe, and Mn in the carbonates could be derived. In this approach the presence of these elements in silicates is neglected. Also the contribution of Mg to the carbonates is not considered, since this element is not measured by the XRF core-scan. For Fe/Al, an overestimation and a poor correlation was found with the laboratory analyses due to the relatively short measurement time of the core scan, insufficient to measure all Al present; it was therefore only used as a qualitative indication for the presence of reactive Fe (not bound to silicate minerals).

Geochemically similar units (GU-I to GU-V) were defined based on the high-resolution core-scan data. Per GU, 5 (GU-II, IV) or 10 (GU-I, II, V) equally distributed subsamples of approximately 30 g were taken from the core. Sampling depths were slightly adjusted only when equidistant sampling forced sampling of 'unreliable intervals', for instance by slumped sediment at the top 10 cm of each 1 m core. Each subsample was oven-dried and homogenized and then equally contributed (5 g or 10 g) to one mixed sample per GU (50 mg). These

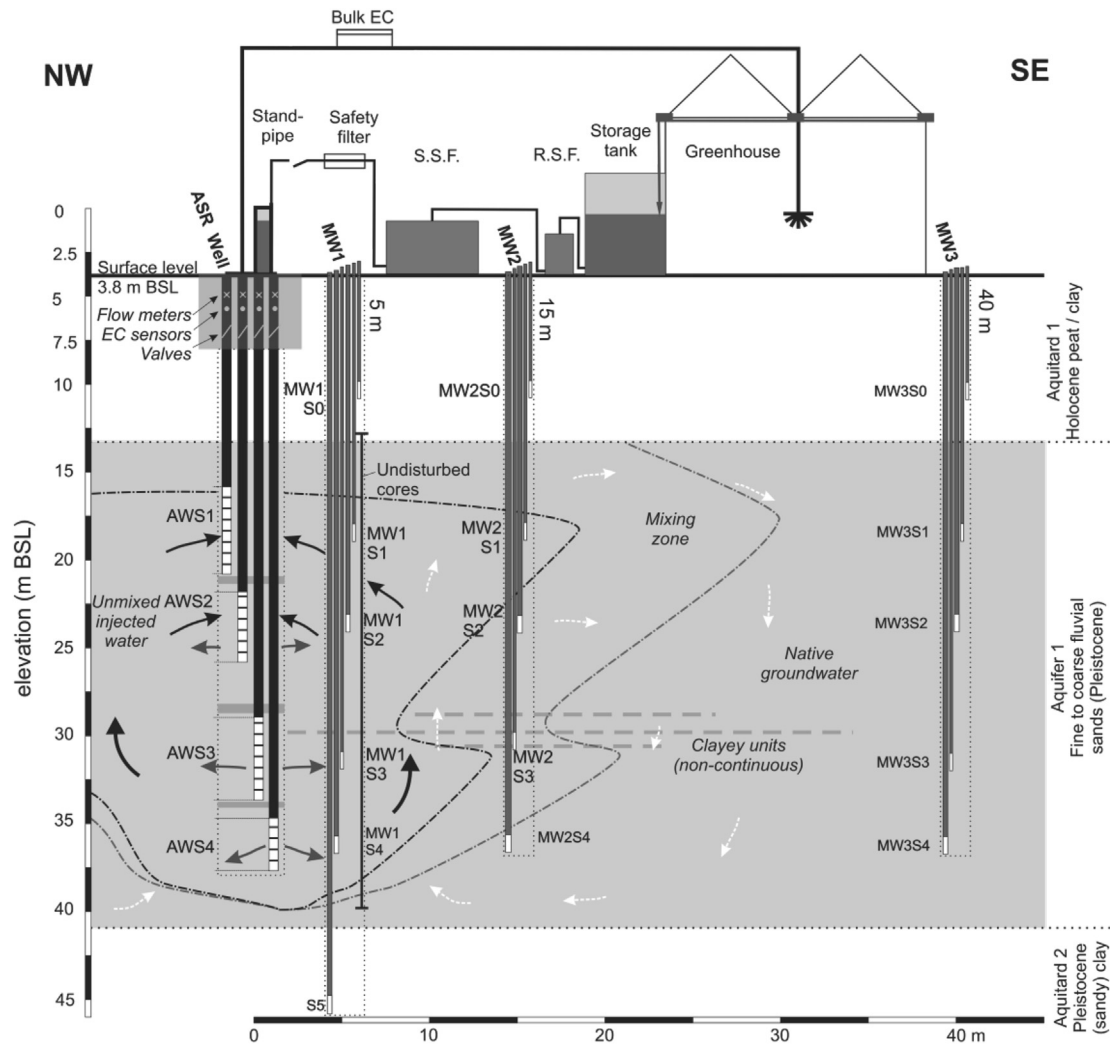


Fig. 1. Cross-section of the Nootdorp ASR system as presented in [Zuurbier et al. \(2014\)](#). Water from the greenhouse is first pre-treated by rapid sand filtration (R.S.F.) and slow sand filtration (S.S.F.) and then injected mainly with the deeper wells (AWS3 and AWS4), whereas most recovery occurred with the shallower wells (AWS1 and AWS2). 'MW' = monitoring well. 'Bulk EC' = EC of the mixed water from all recovering wells. Indicated distribution of the injected water and the flow paths are based on [Zuurbier et al. \(2014\)](#).

mixed samples were analyzed on grain size distribution and SOM and total carbonates using thermogravimetric analysis (TGA). Elemental composition was derived using X-ray fluorescence (XRF), total C and S using LECO Induction Furnace Instruments, and trace elements using

ICP-MS following aqua regia digestion.

2.3.2. (Ground)water sampling

All monitoring wells were sampled prior to ASR operation

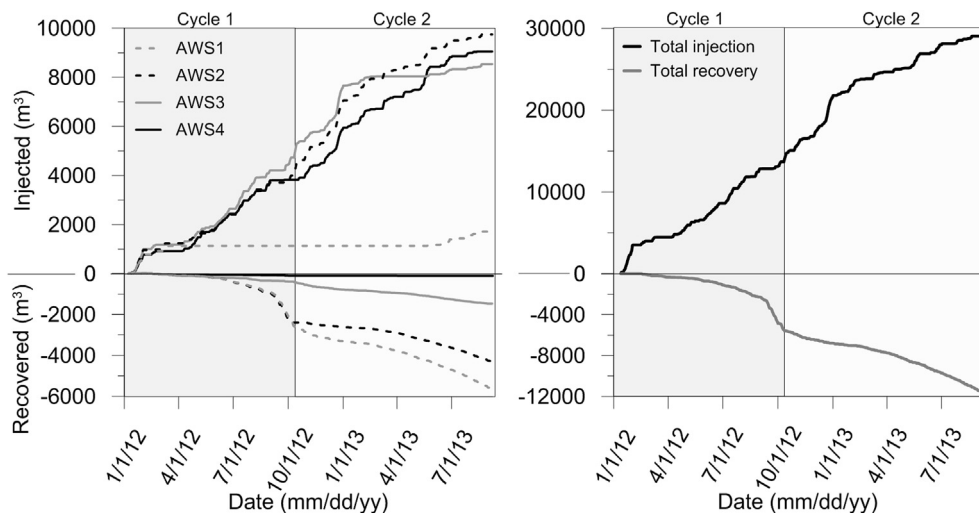


Fig. 2. Operation of the ASR system during the 611 d pilot. Most of the water was injected at AWS2–4, whereas the bulk of the water was recovered by AWS1–2.

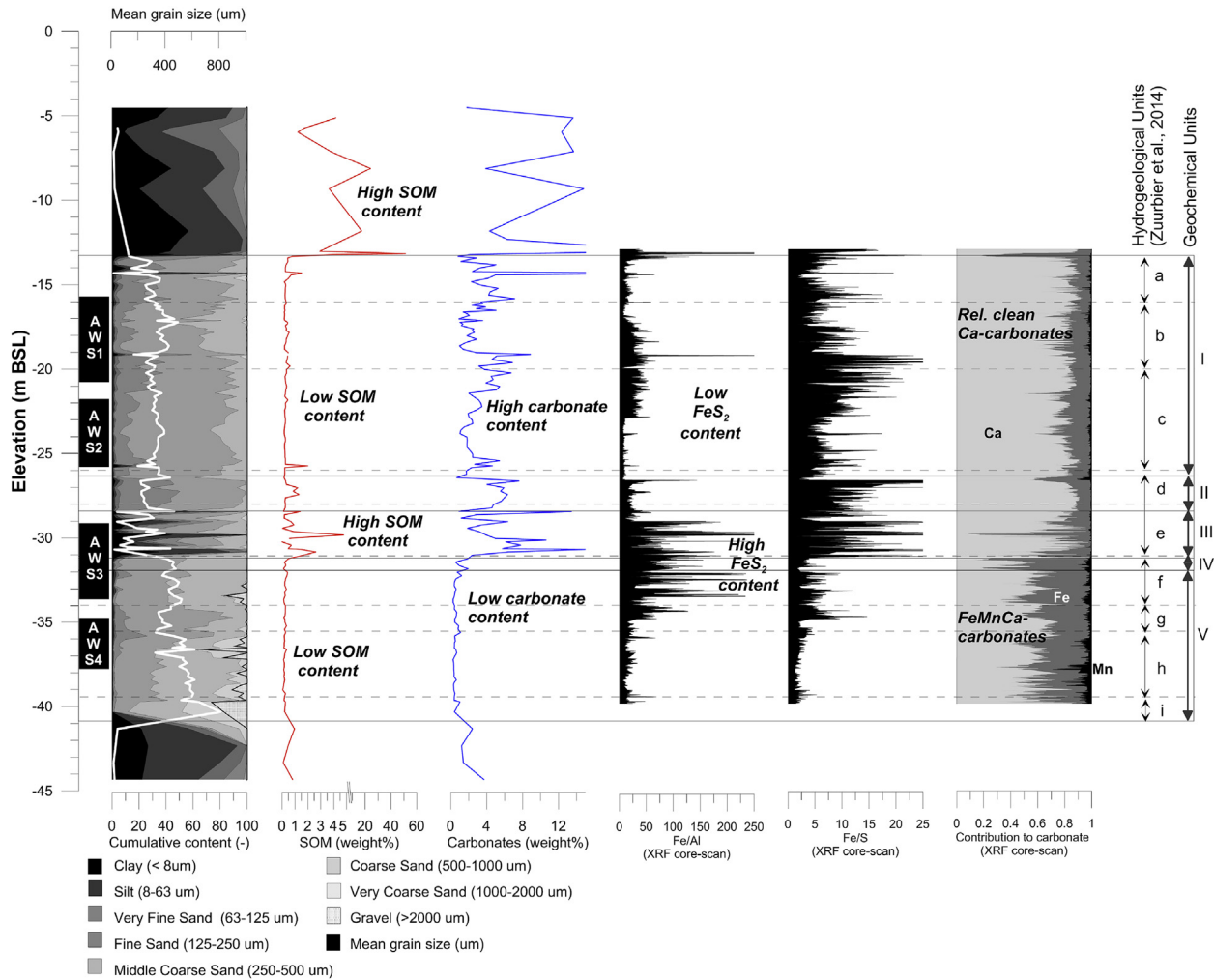


Fig. 3. High-resolution data from physical and chemical sediment analyses and the XRF core-scan at MW1. Fe/Al and Fe/S were derived from the XRF core-scan and indicator for Fe_{TR} (high Fe/Al) and the presence of Fe_{reac} (high Fe/S). Contribution of Ca, Fe, and Mn to the carbonates was based on the XRF core-scan, neglecting silicate-bound elements and the potential presence of Mg (not measured) in the carbonates.

(December 19, 2011). MW1 and MW2 were sampled monthly from January 2012 until September 2013 and a higher frequency was maintained during the first breakthrough of the injected water at MW1 (January/February 2012). Three times the volume of the well riser plus well screen was purged from the wells prior to sampling. The pretreated ASR injection water was sampled 19 times during the pilot runtime. All samples were analyzed in the field in a flow-through cell for EC, pH, temperature, and dissolved oxygen. Samples for lab analysis were passed over a 0.45 μ m cellulose acetate membrane in the field. The reader is referred to Zuurbier et al. (2014) for more information on the handling and analysis of the water samples during the Nootdorp ASR pilot.

2.4. Geochemical and hydrochemical data analysis

2.4.1. Geochemical data analysis

Pyrite content (FeS_2), reactive iron in pyrite (Fe_{py}), total reactive iron (Fe_{TR}), and reactive iron (non-pyrite: Fe_{reac}) were calculated using:

$$FeS_2 = 0.5 \cdot M_{FeS_2} / M_S \cdot S \quad (1.1)$$

$$Fe_{py} = 0.5 \cdot M_{Fe} / M_S \cdot S \quad (1.2)$$

$$Fe_{TR} = 2 \cdot M_{Fe} / M_{Fe_2O_3} \cdot [Fe_2O_3 - 0.1 \cdot Al_2O_3] \quad (1.3)$$

$$Fe_{reac} = Fe_{TR} - Fe_{py} \quad (1.4)$$

where M_{FeS_2} , M_S , and $M_{Fe_2O_3}$ are the molar masses of FeS_2 , S, and Fe_2O_3 , respectively. S is the total S content by weight as measured by the CS elemental analyzer, and Fe_2O_3 and Al_2O_3 are contents by weight, as determined by XRF. The correction of Fe_2O_3 for silicate-bound Fe to determine Fe_{TR} was based on the lowest Fe_2O_3/Al_2O_3 ratio found in the XRF lab analyses (see [Supplementary Information](#)).

The cation exchange capacity (CEC) of each GU was calculated using (Appelo and Postma, 2005):

$$CEC(meq/kg) = 7 \cdot (\%clay) + 35 \cdot (\%C) \quad (2)$$

where %clay is the clay fraction (<2 μ m) derived from the grain size analyses and (%C) is the fraction of organic carbon, which is derived from TGA (assuming %C = %LOI550/2). Total C from the CS analyses was selected only when %C from TGA exceeded the total C from the CS analyzer.

2.4.2. Hydrochemical processes and data analysis

Total dissolved solids (TDS) was calculated based on the

measured concentrations to correct for density differences in the groundwater flow model (Zuurbier et al., 2014). The Base Exchange Index (BEX; Stuyfzand, 1993, 2008) was calculated to identify freshening and salinization.

The potentially relevant hydrochemical reactions are shown in Table 1. Since NO_3^- concentrations in rainwater are low, DO is considered the most relevant oxidant in the injection water. Some processes (cation exchange, nitrification, oxidation of adsorbed Fe and Mn) are mainly relevant in the mixing zone and during freshening, but rarely during later injection, while others (pyrite and SOM oxidation, carbonate dissolution) are relatively persistent, or relevant during recovery (MnO_2 and $\text{Fe}(\text{OH})_3$ reduction, cation exchange).

The amount of pyrite oxidation was calculated using the maximum SO_4 -production observed at the different ASR well screens and was based on the difference between SO_4^{2-} concentration in the injected and recovered water. The amount of oxygen consumption by pyrite was calculated as:

$$\Delta C(\text{O}_{2(\text{pyrite})}) = \frac{3.75}{2} \cdot [C(\text{SO}_4) - C(\text{SO}_{4(\text{injection})}) - C(\text{SO}_{4(\text{NO}_3)})] \quad (3)$$

where $\Delta C(\text{O}_{2(\text{pyrite})})$ is the oxygen consumption by pyrite, $C(\text{SO}_4)$ is the molal concentration SO_4^{2-} observed in the aquifer upon injection, $C(\text{SO}_{4(\text{injection})})$ is the molal SO_4^{2-} concentration in the injection water, and $C(\text{SO}_{4(\text{NO}_3)})$ is the molal SO_4 -production from NO_3^- (assuming all NO_3^- is consumed by oxidation of pyrite). The latter was calculated using:

$$C(\text{SO}_{4(\text{NO}_3)}) = \frac{10}{14} [C(\text{NO}_{3(\text{injected})}) - C(\text{NO}_3)] \quad (4)$$

where $C(\text{NO}_{3(\text{injected})})$ is the molal concentration of NO_3^- in the injection water (0.05 mmol/L in the collected rainwater) and $C(\text{NO}_3)$ is the molal concentration of NO_3^- observed in the aquifer during storage.

2.5. Modelling codes and set-up

A reactive transport model was built to verify if alternating freshening and salinization could indeed affect the recovered water quality and explore long-term effects and the effect of injection water modification.

2.5.1. Input flow model

SEAWAT (Langevin et al., 2007) was used to calculate the flow field in an axi-symmetrical model during the two field trial cycles (611 days, January 2012 – September 2013). Three subsequent fictitious cycles were added in a simplified way after Cycle 2. TDS was used to calculate the density in each cell, as described in Zuurbier et al. (2014). The modelled pumping scheme is described in Table 3. The three additional cycles contained relatively long periods without injection, resulting in more salinization at the end of each cycle than in Cycle 1 and 2. Pre- and post-processing was performed using PMWIN8.06 (Simcore Software, 2010).

2.5.2. PHT3D model input for reactive transport (cation exchange)

Initial concentrations of Na^+ , Cl^- , Ca^{2+} , Mg^{2+} , K^+ , NH_4^+ , HCO_3^- , and the pH were derived from chemical analyses on samples taken at MW1 prior to ASR operation. The exchanger compositions (Na-X , Ca-X , Mg-X , K-X , $\text{NH}_4\text{-X}$) were first calculated by PHREEQC (Parkhurst and Appelo, 1999) batch calculations using the standard PHREEQC database and the initial concentration and CEC at the levels of the MW1 well screens. The conversion of CEC-values to meq/l for PHREEQC was performed assuming a grain density of 2650 kg/m³ and the porosity of the target aquifer (0.25–0.35) derived from the breakthrough of Cl^- (Zuurbier et al., 2014). A porosity of 0.4 was assumed to calculate the CEC for the confining clay units. The approach discarded some of the geochemical variation found centrally in the target aquifer where MWs were absent (the locally clayey intervals: GU-II and GU-III). The exchanger composition and the calcite content (derived from TGA and assuming all carbonates to be present as calcite) of each cell (converted to attain moles per liter of bulk aquifer volume) were corrected for the axi-symmetry of the model (Wallis et al., 2013). Equilibrium conditions were assumed for calcite, redox process were not included. This provided an efficient and robust model that included the simulation of freshening and salinization effects in addition to the effects of density-driven flow on water quality development in the target aquifer.

To evaluate the influence of the CEC, injection water composition, and flow patterns on water quality development regarding Na^+ , four additional scenarios were run:

1. A scenario in which GU-III was introduced as a continuous horizontal layer with its potentially high CEC, which was based on geochemical analyses at MW1 (Table 1).

Table 1

Potentially relevant hydrochemical reactions involved with the injection of oxic rainwater in the deeply anoxic, brackish target aquifer.

Process	Reaction equation
Pyrite oxidation	
Pyrite-oxidation by O_2	$3.75\text{O}_2 + \text{FeS}_2 + 3.5\text{H}_2\text{O} \rightarrow \text{Fe}(\text{OH})_3 + 2\text{SO}_4^{2-} + 4\text{H}^+$
Pyrite-oxidation by NO_3^-	$14\text{NO}_3^- + 5\text{FeS}_2 + 4\text{H}^+ \rightarrow 5\text{Fe}^{2+} + 10\text{SO}_4^{2-} + 7\text{N}_2 + 2\text{H}_2\text{O}$
Other redox	
Oxidation of organic matter by O_2	$\text{O}_2 + \text{CH}_2\text{O} \rightarrow \text{CO}_2 + \text{H}_2\text{O}$
Oxidation of organic matter by NO_3^-	$\text{NO}_3^- + 1.25\text{CH}_2\text{O} \rightarrow 0.5\text{N}_2 + \text{HCO}_3^- + 0.75\text{H}_2\text{O} + 0.25\text{CO}_2$
Fe-carbonate oxidation	$0.25\text{O}_2 + \text{FeCO}_3 + 1.5\text{H}_2\text{O} \rightarrow \text{Fe}(\text{OH})_3 + \text{CO}_2$
Mn-carbonate oxidation	$0.5\text{O}_2 + \text{MnCO}_3 \rightarrow \text{MnO}_2 + \text{CO}_2$
Oxidation of Fe^{2+}	$\text{Fe}^{2+} + 0.25\text{O}_2 + 2.5\text{H}_2\text{O} \rightarrow \text{Fe}(\text{OH})_3 + 2\text{H}^+ (\text{dissolved Fe}^{2+})$
	$\text{Fe-X}_2 + 0.25\text{O}_2 + \text{CaCO}_3 + 1.5\text{H}_2\text{O} \rightarrow \text{Ca-X}_2 + \text{Fe}(\text{OH})_3 + \text{CO}_2 (\text{adsorbed Fe}^{2+})$
	$\text{Mn}^{2+} + 0.5\text{O}_2 + \text{H}_2\text{O} \rightarrow \text{MnO}_2 + 2\text{H}^+ (\text{dissolved Mn}^{2+})$
	$\text{Mn-X}_2 + 0.5\text{O}_2 + \text{CaCO}_3 \rightarrow \text{Ca-X}_2 + \text{MnO}_2 + \text{CO}_2 (\text{adsorbed Mn}^{2+})$
	$\text{Fe}(\text{OH})_3 + 0.25\text{CH}_2\text{O} + 1.75\text{CO}_2 \rightarrow \text{Fe}^{2+} + 2\text{HCO}_3^- + 0.75\text{H}_2\text{O}$
	$2\text{Fe}^{2+} + \text{MnO}_2 + 4\text{H}_2\text{O} \rightarrow 2\text{Fe}(\text{OH})_3 + \text{Mn}^{2+} + 2\text{H}^+$
	$\text{MnO}_2 + 0.5\text{CH}_2\text{O} + 1.5\text{CO}_2 + 0.5\text{H}_2\text{O} \rightarrow \text{Mn}^{2+} + 2\text{HCO}_3^-$
	$4\text{O}_2 + 2\text{NH}_4^+ \rightarrow 2\text{NO}_3^- + 2\text{H}_2\text{O} + 4\text{H}^+$
Dissolution	
Carbonate dissolution	$2\text{H}^+ + (\text{Ca, Fe, Mn})\text{CO}_3 \rightarrow (\text{Ca, Fe, Mn})^{2+} + \text{CO}_2 + \text{H}_2\text{O} (\text{proton-buffering})$
	$\text{CO}_2 + (\text{Ca, Fe, Mn})\text{CO}_3 + \text{H}_2\text{O} \rightarrow (\text{Ca, Fe, Mn})^{2+} + 2\text{HCO}_3^- (\text{following CO}_2\text{-production})$
Cation exchange	
Freshening	$a\text{Ca}^{2+} + [\text{bNa, cMg, dK, eNH}_4, \text{fFe, gMn}] - \text{X} \rightarrow \text{bNa}^+ + \text{cMg} + \text{dK} + \text{eNH}_4 + \text{fFe} + \text{gMn} + [\text{aCa}] - \text{X}$
Salinization	$\text{bNa}^+ + \text{cMg} + \text{dK} + \text{eNH}_4 + \text{fFe} + \text{gMn} + [\text{aCa}] - \text{X} \rightarrow \text{aCa}^{2+} + [\text{bNa, cMg, dK, eNH}_4, \text{fFe, gMn}] - \text{X}$

Table 2
Modeled ASR cycles in this study. Distribution of pumping rates (Q_{tot}) over the MPPW screens (S1 / S2 / S3 / S4) in the added cycles is given in percentages between brackets.

ASR phase	Stress periods	Pumping	Duration (d)
Cycle 1	1–37	As recorded by flowmeters (Fig. 2)	273
Cycle 2	38–83	As recorded by flowmeters (Fig. 2)	338
Idle Cycle 2	84	Idle	30
Injection Cycle 3–5	85, 89, 93	$Q_{\text{tot}} = 133.3 \text{ m}^3/\text{d}$ (0% / 10% / 40% / 50%)	150
Storage Cycle 3–5	86, 90, 94	Idle	30
Recovery Cycle 3–5	87, 91, 95	$Q_{\text{tot}} = -53.3 \text{ m}^3/\text{d}$ (60% / 40% / 0% / 0%)	150
Idle Cycle 3–4	88, 92	Idle	35

2. A scenario with three times higher CECs for each hydro-geological unit (which was still within a realistic range according to Breeuwsma et al. (1986)) in the whole target aquifer to assess the sensitivity to CEC;
3. A scenario with addition of 5 mmol/l gypsum (CaSO_4) to the injection water to test the accelerated release of Na^+ from the exchanger during freshening;
4. A scenario in which a fully penetrating well is used, but buoyancy and seepage are neglected. This way, the results of the MPPW can be compared with a conventional, bi-directional ASR

system. The CEC was again raised by a factor 3 to emphasize the effect of cation exchange.

3. Results

3.1. Target aquifer properties

3.1.1. Geochemical aquifer characterization

The extensive geochemical analyses produced a solid understanding of the aquifer geochemical properties. The following reactive phases were identified (Fig. 3, Table 2):

Table 3
Geochemical properties of the target aquifer for the five geochemical units (GU-I–V).

Parameter	Unit	GU-I	GU-II	GU-III	GU-IV	GU-V
Depth	m BSL	13.16–26.57	26.57–28.42	28.42–31.12	31.12–31.82	31.82–41.32
Clay fraction (<2 μm)	% d.w.	0.69	0.77	4.75	0.66	0.51
Gravel fraction (>2 mm)	% d.w.	0.00	0.00	0.00	0.00	4.15
SOM	% d.w.	0.41	0.51	1.02	0.27	0.22
Carbonates	% d.w.	4.38	5.32	4.90	0.82	0.44
Total C	% d.w.	0.56	0.69	1.25	0.07	0.07
CEC-calculated	meq/kg	12.0	14.3	51.1	7.1	6.0
Pyrite	% d.w.	0.06	0.09	1.05	0.90	0.28
Fe(total)	% d.w.	0.55	0.71	1.75	0.86	0.40
Fe(pyrite)	% d.w.	0.03	0.04	0.49	0.42	0.13
Fe (TR)	% d.w.	0.13	0.28	0.91	0.47	0.15
Fe(react, non-pyrite)	% d.w.	0.10	0.24	0.42	0.05	0.02
MnO	% d.w.	0.1	0.2	0.3	0.1	<0.1
As	ppm	2.2	2.3	14.2	6.1	4.0

Table 4
Groundwater quality observed in the Nootdorp target aquifer, average quality of the injected and recovered water, and most relevant water quality limits.

Parameter	Unit	Ambient groundwater MW1				Injection	Average recovery	Quality limits
		S1	S2	S3	S4	AW	AW	
Nr. of samples:	n	1	1	1	1	19	99	
EC-20	$\mu\text{S}/\text{cm}$	1448	2177	3159	4062	72	151	250 ^N , 2500 ^D
Temp	$^{\circ}\text{C}$	10.6	10.5	10.3	10.5	10.4	14.1	
pH	(–)	6.9	7.0	7.0	7.0	7.5	7.9	
DO	mmol/l	0.00	0.00	0.00	0.00	0.32*	0.04	
Na^+	mmol/l	6.6	12.0	19.70	25.8	0.1	0.14	0.5 ^N , 8.7 ^D
K^+	mmol/l	0.3	0.4	0.6	0.9	0.01	0.02	
Ca^{2+}	mmol/l	4.0	4.5	5.4	7.0	0.23**	0.71	
Mg^{2+}	mmol/l	0.8	1.3	2.0	2.8	0.02	0.05	
Fe^{2+}	$\mu\text{mol}/\text{l}$	469	335	245	258	0.2	0.41	3.6 ^{N,D}
Mn^{2+}	$\mu\text{mol}/\text{l}$	19	19	22	30	0.1	2.0	0.9 ^{N,D}
NH_4^+	mmol/l	1.2	1.6	1.2	1.0	0.0	0.1	0.03 ^D
SiO_2	mmol/l	0.8	0.8	0.7	0.7	0.0	0.06	
Cl^-	mmol/l	3.2	10.0	21.3	27.6	0.1	0.11	7.1 ^D
SO_4^{2-}	mmol/l	0.0	0.0	0.0	0.0	0.03	0.12	2.6 ^D
TIC	mmol/l	14.4	17.3	21.0	21.1	0.6	1.32	
NO_3^-	mmol/l	0.0	0.0	0.0	0.0	0.05	0.02	
$\text{PO}_4\text{-t}$	mmol/l	0.06	0.06	0.06	0.05	0.00	0.00	
As-t	$\mu\text{mol}/\text{l}$	0.02	0.02	0.00	0.00	0.00	0.05	0.13
DOC	mmol/l	0.4	0.9	1.0	0.5	0.1	–	
BEX	(–)	5.0	4.2	1.5	2.8	0.0	0.13	
SI (calcite)	(–)	0.3	0.5	0.6	0.6	–2.2	–0.99	
SI (siderite)	(–)	1.9	1.9	1.8	1.8	–2.7	–1.98	

^NSpecific water quality limits horticulture at the Nootdorp ASR site.

^DDrinking water limits (EU drinking water directive 98/83/EG, 1998).

*DO range observed: 0.21–0.41 mmol/l.

**Ca range observed: 0.08–0.47 mmol/l.

- Carbonates are present mainly in the upper GU's (I–III; ~5% weight) and less in the deeper GU-IV and V (<1% weight). The XRF core-scan results indicated however that the carbonates in the deeper units are potentially enriched with Fe (up to 50%) and Mn (up to 20%), while Ca is the dominant cation in the carbonates in GU-I–III (generally >85%), indicating a relatively pure calcite composition;
- The pyrite content is relatively low at the shallow GU-I and II and high in the central (GU-III and IV: 0.90–1.05% weight) and deeper intervals (GU-IV: 0.28% weight);
- Sedimentary organic matter (SOM) is present throughout the target aquifer, although its content is lowest in GU-IV and V (0.22–0.27% weight) and highest in GU-III (1.02% weight);
- The derived CECs (Table 3) are relatively low and in line with CECs observed for this fluvial sediment type (Van Helvoort, 2003).

3.1.2. Native groundwater and injection water quality

The native groundwater is marked by a clear salinity stratification, with relatively freshwater at the aquifer top and brackish water at the base (Table 4). A positive BEX index indicates relatively recent freshening of the aquifer. Deeply anoxic conditions in the native groundwater are reflected by the absence of DO, NO_3^- , and SO_4^{2-} (Table 4), as well as by the high CH_4 -concentrations reported for this aquifer (Fortuin and Willemsen, 2005; Stuyfzand, 1994).

The injection water was oxic and had low concentrations of NO_3^- and SO_4^{2-} . Low concentrations of Ca^{2+} and HCO_3^- resulted from dissolution of calcite in the slow sand filter (Table 4). The salinity of the injection water exceeded 0.25 mmol/l when precipitation coincided with strong western winds (mainly in Autumn, Winter). Since rainwater from Spring and Summer was the first water to be recovered, the average salinity of the recovered water was lower than in the average injection water. The assimilable organic carbon (AOC, 10 $\mu\text{g/l}$) and total suspended solids concentrations (TSS, <1 mg/l) were low, indicating a low risk of well clogging (Russell, 2013), which was confirmed by a constant specific capacity during 20 months of operation.

3.2. The behavior of Na^+ during MPPW-ASR

3.2.1. Observed trends in Na^+ concentrations

While the transport of Cl^- was conservative (Zuurbier et al., 2014), observations at 5 m from the ASR well (MW1; see Supplementary Information) showed enrichment with Na^+ and other cations from the ambient groundwater during injection. At the recovery wells (AWS1, AWS2), an earlier arrival of Na^+ at significantly higher concentrations compared to Cl^- was observed during the final recovery phases of Cycle 1 (Fig. 4). In Cycle 2, Na^+ concentrations in unmixed recovered water were constantly higher than Cl^- concentrations at AWS1, but equal at AWS2, and actually lower during salinization at AWS3 (Fig. 4). In Fig. 5, the Na^+ and Cl^- concentrations are plotted on different axes to indicate the relative increase/decrease of Na^+ .

3.2.2. Assessment of the role of cation exchange on Na^+ during MPPW-ASR

3.2.2.1. Reproduction of field observations by the PHT3D-model and simulation of subsequent cycles. PHREEQC calculations to derive the exchanger composition showed that no more than 11% of the exchanger was occupied by Na^+ even at the base of the aquifer, while Ca^{2+} occupied 53–81% of the exchanger sites. The straightforward modelling could reproduce the trends observed at the ASR wells: Na^+ concentrations at AWS1 were almost continuously

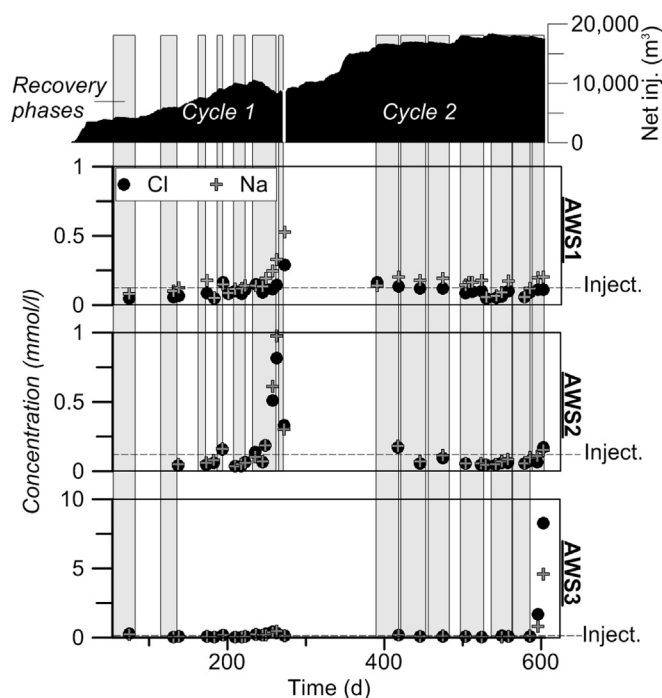


Fig. 4. Observed Cl^- and Na^+ concentrations at the upper ASR wells (AWS1 – AWS3, where the recovery occurred) during two subsequent ASR cycles (2012–2013). A relatively small volume was recovered at AWS3; the bulk of the freshwater was recovered at AWS1 and AWS2 (Fig. 2). The 'net injected' volume is calculated using: gross volume(injected) minus gross volume(recovered). 'Inject' marks the average injection concentration.

elevated with respect to Cl^- (Fig. 6), reaching concentrations around and eventually exceeding 0.5 mmol/l. This limit was not exceeded (Cycle 3) or exceeded 45 days later (Cycle 4 and 5; almost one-third of the total recovery period later) when solely Cl^- was analyzed. The Na^+ concentrations at AWS2 produced by the PHT3D-model were significantly lower compared to Cl^- during salinization at the end of recovery periods (Fig. 6b: Cycle 3–5),

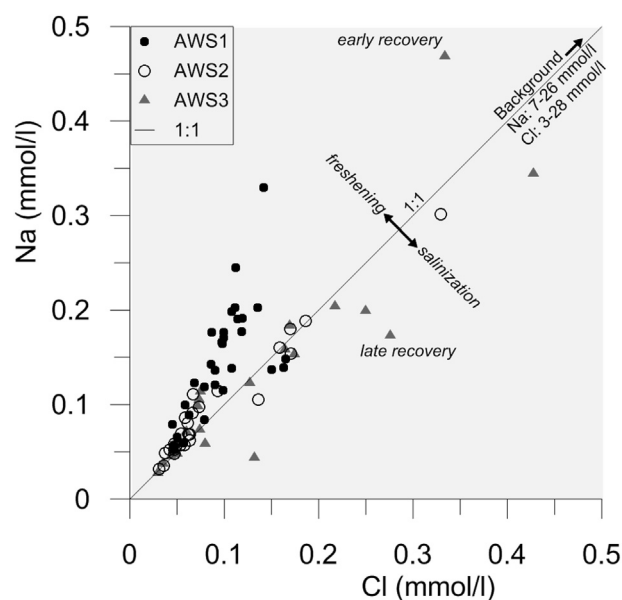


Fig. 5. Na^+ versus Cl^- indicating that freshening (resulting in concentrations $\text{Na} > \text{Cl}$) and salinization (resulting in concentrations $\text{Na} < \text{Cl}$) occurred before injected water was recovered at the various wells screens of the MPPW.

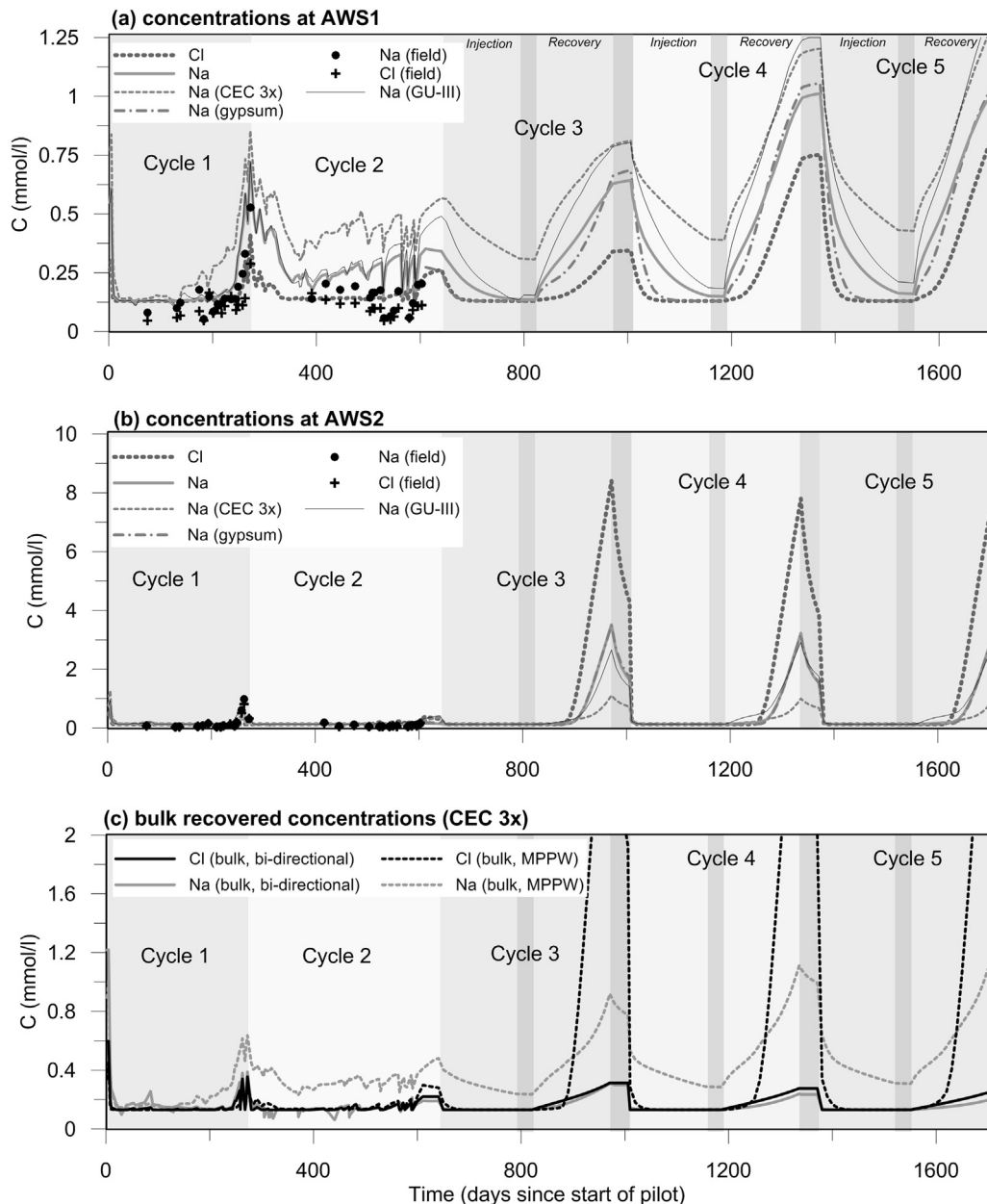


Fig. 6. Observed and modelled Na^+ and Cl^- concentrations by PHT3D for the recovery wells AWS1 (a) and AWS2 (b). The modelled concentrations for the bulk recovered water quality assuming a 3 times elevated CEC (c), which can be compared with conventional bi-directional ASR (no buoyancy). Modelling results for an elevated CEC (3 times the CEC derived from aquifer sediments) and a case with injection water enriched with 5 mmol/l gypsum (CaSO_4) are shown in (a) and (b) to demonstrate their consequences. Only Cycle 3–5 is shown for the gypsum enrichment for the sake of clarity and coincides with 'Na' (no enrichment) in (b). Na (GU-III) = scenario with a high CEC at GU-III (51 meq/kg, Table 3).

comparable with the field observations at AWS3 (Fig. 4). The recovery at AWS2 could therefore be extended with approximately 30 days.

When GU-III was introduced with its high CEC (51.1 meq/kg), a significant and continuous surplus of Na^+ was observed especially at MW1S2 and MW1S3 (results not shown) and to a lesser extent at AW1S1 (Fig. 6a,b). A high-CEC unit centrally in the target aquifer would have had a negative effect: concentrations at AWS1 would rapidly exceed 0.5 mmol/l (comparable to the high CEC scenario), without sufficient compensation by Na^+ retardation.

3.2.2.2. Implications of cation exchange for Na^+ in the bulk recovered water. The results show that bulk Na^+ concentrations are elevated with respect to Cl^- in the bulk recovered water at the start of

recovery periods for an MPPW-ASR system (Fig. 6c). Na^+ concentrations never reach the injected concentration. Bulk Na^+ concentrations are lower than Cl^- concentrations in the recovered water during later stages of recovery due to the retarded arrival at AWS2. For a theoretical ASR-system with bi-directional flow paths (no buoyancy) in the same aquifer it was found that water quality will improve with consecutive cycles (Fig. 6c).

3.2.2.3. Effect of sediment and injection water composition on Na^+ in the recovered water. A higher CEC in the target aquifer results in higher Na^+ concentrations at AWS1 (Fig. 6a). The reverse effect was again observed at AWS2, yet stronger than with the 3 times lower field CEC. Here, Na concentrations were generally <0.5 mmol/l, although Cl^- concentrations reached 8 mmol/l.

Addition of 5 mmol/l gypsum while assuming the low field CECs would lower Na^+ concentrations at AWS1 in the first phase of recovery, but could not increase the recovered water volume with sufficiently low Na^+ concentrations. In this case, the Na^+ concentrations were relatively higher at the top of the AWS1 well screen and lower at its base, but the recovered water quality was similar. Raising the addition of gypsum to 20 mmol/l did not result in improvement of the recovered water quality, nor an increase in Na^+ retardation.

3.3. Concentration increases for Fe^{2+} , Mn^{2+} , and As

3.3.1. Observed trends in Fe^{2+} , Mn^{2+} , and As concentrations

During recovery in Cycle 1, Mn^{2+} concentrations frequently exceeded the operational limit of 0.9 $\mu\text{mol/l}$ at AWS1 (which was a recovery well after injecting 1132 m^3). Breakthrough of also Fe^{2+} and As was observed here later during recovery. At AWS2 (alternating injection/recovery), Mn^{2+} and Fe^{2+} concentrations were significantly lower: an increase of Mn^{2+} was observed only during the first, short recovery stages and at the end of Cycle 1. AWS3 was used mainly for injection and showed high Mn^{2+} and As concentrations during short recovery stages.

In Cycle 2, high Mn^{2+} and elevated Fe^{2+} and As concentrations were observed at AWS1, but concentrations were lower than in Cycle 1, and were lowered further after partly restoring the freshwater injection at this well. The recovered water at AWS2 was virtually free of As, Fe^{2+} , and Mn^{2+} in Cycle 2. Mn^{2+} and later Fe^{2+} did cause frequent and severe deterioration of the water recovered at AWS3, despite a significant net injection. Most enrichment was observed at the S3 wells (also at MW1, see [Supplementary Information](#)) and concerns Mn^{2+} . The As mobilization tended to decrease over time. Water reaching AWS1, which was injected at deeper aquifer intervals, was on average slightly enriched with all elements of concern.

3.3.2. Assessment of the mobilization of Fe^{2+} and Mn^{2+}

3.3.2.1. Effect of mixing and cation exchange on Fe^{2+} and Mn^{2+} . Mixing was assessed with the mixing lines for Fe^{2+} and Mn^{2+} in [Fig. 8](#). Only at MW1, a part of the observed concentrations plot on the mixing line. A relation with the BEX was partly present for Fe^{2+} , but not for Mn^{2+} (see [Supplementary Information](#)). Enrichment of Fe^{2+} and Mn^{2+} ($\sim 3 \mu\text{mol/l}$) occurred even in freshwater samples with a neutral BEX (freshening completed).

3.3.2.2. Effects of carbonate dissolution in combination with pyrite oxidation. The geochemical analyses ([Fig. 3](#)) indicated a potential presence of Fe- and Mn-bearing carbonates at the S3 and S4 levels. However, the dominance of the more soluble calcite (CaCO_3) should primarily result in an increase in Ca^{2+} and inorganic carbon (primarily HCO_3^- under the pH observed ([Appelo and Postma, 2005](#))). The increase in Ca^{2+} ([Fig. 9](#)) was generally accompanied by an increase in HCO_3^- with a $\pm 1:2$ ratio ($\text{Ca}:\text{HCO}_3$, [Table 1](#)), representing calcite equilibrium under varying CO_2 pressures (from atmospheric ($p\text{CO}_2 = 10^{-3.5}$ atm) up to around $10^{-2.4}$ atm). Relatively low Ca^{2+} concentrations were accompanied by a relatively high positive BEX. Relatively high Ca^{2+} concentrations at the S3-level (generally accompanied by only a slightly positive BEX) on the other hand indicated calcite-dissolution by proton-buffering upon pyrite-oxidation ([Hartog et al., 2002; Stuyfzand, 1998](#)). One sample indicated salinization (negative BEX), which may explain its relatively high Ca^{2+} concentration ([Fig. 9](#)).

To verify which reactive processes were driving the carbonate dissolution observed, simple PHREEQC batch simulations were performed. The injection water's ionic balance was first attained by adjusting the HCO_3^- concentration, than equilibrated under

Table 5

O_2 consumption by pyrite based on SO_4 -production found at MW1 at the end of long periods of injection.

MW	O_2 consumed by pyrite oxidation	
	Cycle 1	Cycle 2
S1	48%	33%*
S2	18%	23%
S3	58%	108%
S4	68%	98%

*Based on SO_4 concentrations observed at AWS1 during recovery after injecting small volumes of freshwater.

atmospheric $p\text{CO}_2$, subsequently brought in equilibrium with calcite in a closed system, and finally all dissolved oxygen was used to oxidize pyrite while maintaining the calcite equilibrium (see reaction equations in [Table 1](#)). The equilibration dissolution resulted in a relatively low Ca^{2+} concentration (0.27 mmol/l), close to the lowest Ca^{2+} concentration observed in the recovered freshwater ([Fig. 9](#)). The PHREEQC simulation indicated no more than 0.61 mmol Ca/l and 0.91 mmol HCO_3^- /l could be attained when pyrite oxidation by oxygen in the average injection water was stimulating carbonate dissolution. The sporadically observed higher DO (up to 0.4 mmol/l), Ca^{2+} (up to 0.47 mmol/l), and HCO_3^- (up to 0.95 mmol/l) concentrations in the injection water could not have led to the Ca^{2+} and HCO_3^- concentrations observed, especially in Cycle 1 ([Fig. 9](#)).

The calculated oxygen consumption ([Table 5](#)) based on the observed SO_4 -production indicated that virtually all oxygen in the injected water at the lower part of the aquifer (GU-IV and V, level S3

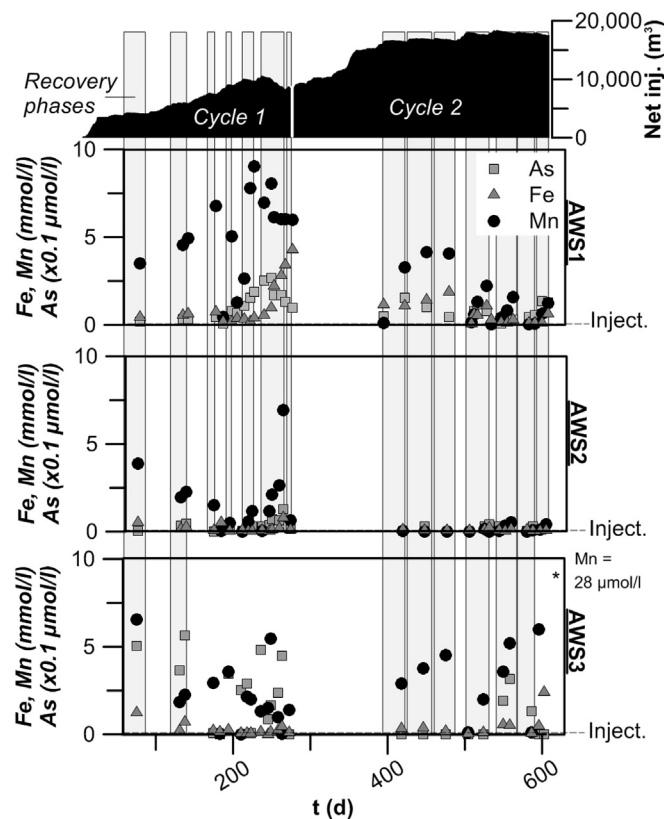


Fig. 7. Concentrations of Fe, Mn, and As in the water recovered from the recovery wells (AWS1 – AWS3) during two subsequent ASR cycles (2012–2013). Recovery at AWS3 was relatively limited; the bulk of the freshwater was recovered at AWS1 and AWS2 ([Fig. 2](#)). Inject. = concentration in the injection water. 'Net inj.' volume is the net injected volume and calculated using: gross volume(injected) minus gross volume(recovered).

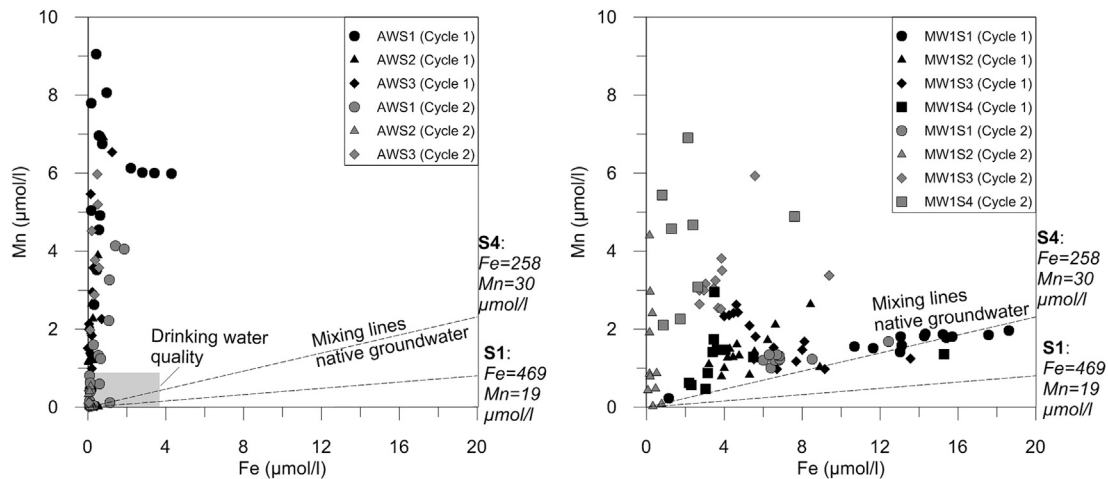


Fig. 8. Mn versus Fe recovered from the ASR well (AW) and observed in the aquifer at 5 m from the ASR well (MW1).

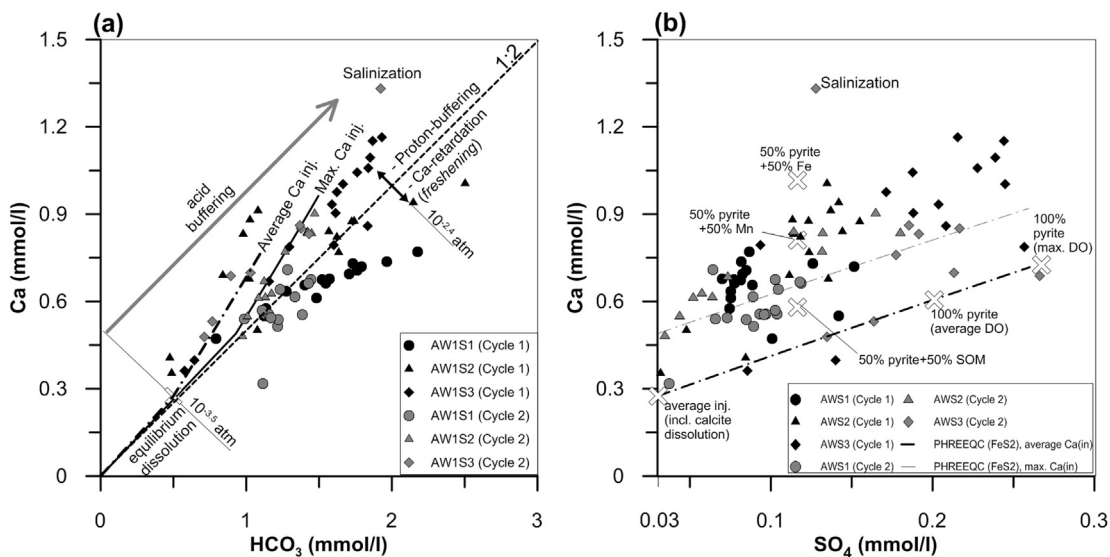


Fig. 9. Ca^{2+} versus HCO_3^- (a) and Ca^{2+} versus SO_4^{2-} concentrations (b) in the water recovered from the ASR wells. The dashed line in (a) represents calcite equilibrium for increasing CO_2 -pressure, the calculated concentrations as a consequence of pyrite oxidation are marked for the average and the maximum observed Ca^{2+} concentrations in the injection water.

and S4) was used for oxidation of pyrite in Cycle 2 (Table 5), but not in Cycle 1. Furthermore, the $\text{Ca}:\text{SO}_4$ -ratio at the S3-level was lower in Cycle 2 than in Cycle 1 (Fig. 8b).

3.3.2.3. Removal of mobilized Fe and Mn by adjustments in the injection scheme. To improve the recovered water quality at AWS1, periodic injection of small rainwater volumes was applied to stimulate subsurface iron removal (SIR; Van Beek, 1985; van Halem et al., 2011) during Summer 2013 after 1 year of only recovery at this well. The Mn^{2+} concentrations decreased from 4.1 $\mu\text{mol/l}$ to almost 0 $\mu\text{mol/l}$. About 8 vol of water could subsequently be recovered with Mn^{2+} concentrations below the limit (0.9 $\mu\text{mol/l}$) after injection of 1 volume of oxygen-containing rainwater (see Fig. 7 and the Supplementary Information). Fe^{2+} was kept below 1 $\mu\text{mol/l}$. The SO_4 -production during SIR injections following abstraction of Mn^{2+} and Fe^{2+} -rich water at S1 level was lower in Cycle 2 (Table 5). Removal of As by SIR appeared less effective.

4. Discussion

4.1. Increasing Na^+ concentrations during MPPW-ASR in coastal aquifers

Field observations and reactive transport modelling demonstrated a dominance of cation exchange during MPPW-ASR in controlling Na^+ mobility. MPPW-ASR optimizes the recovery of practically unmixed water (low EC, no increase in Cl^-), but repeated salinization of the deeper aquifer intervals during ASR cycles resulted in non-conservative arrival of Na^+ (and other cations from the native groundwater like Mg^{2+} , K^+ , Fe^{2+} , Mn^{2+}) at the recovery wells. Since particularly a zone of Na^+ -enriched water is undesirable for irrigation water use, the control of Na^+ concentrations cation exchange processes was a critical factor during the MPPW-ASR pilot.

A cycle-after-cycle water quality improvement is lacking around the deepest wells screens during MPPW-ASR thanks to a repeating

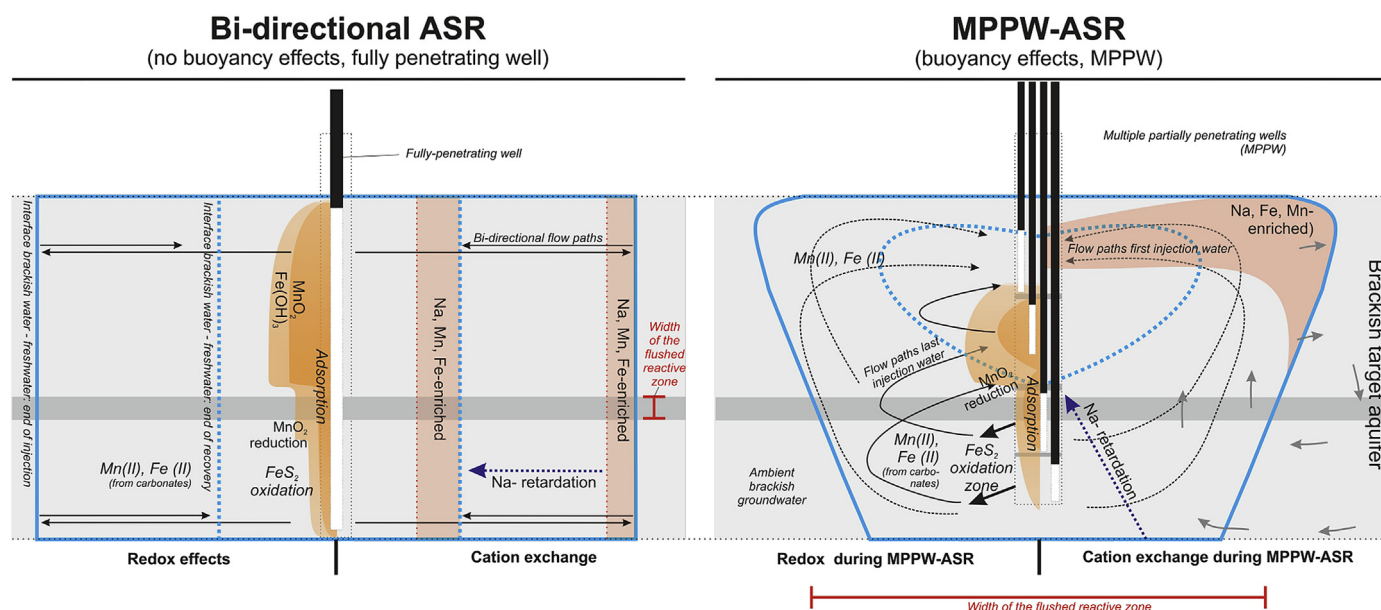


Fig. 10. Conceptualization of reactive transport processes occurring during the Nootdorp MPPW-ASR pilot, as compared to bi-directional ASR. Also the flushed width of a hypothetical reactive zone in the middle of the aquifer during for both ASR flow regimes is illustrated.

cycle of Na^+ adsorption (recovery: brackish water replaces infiltrated freshwater) and desorption (injection: freshwater replaces brackish water). Modelling showed that a zone with a CaCl_2 water type around the freshwater body cannot decrease Na^+ -enrichment, as it is diluted and then transported to the shallower parts of the aquifer by density-driven flow, while a native, brackish NaCl water type continues to encroach the deeper part (Fig. 10).

The net positive or negative effect of Na^+ mobility on the RE depends on the combination of the CEC, native groundwater and injection water composition, and the limits set for Na^+ in the recovered water. The mass of mobilized Na^+ will increase with increasing CEC and native water salinity. The volume of the enriched zone and its Na^+ concentration will be controlled by Ca^{2+} concentrations in the injected water. The potential water quality deterioration should be taken into account especially in saline, anisotropic aquifers with intercalated fine sand beds (with a high CEC), which may be preferably targeted over coarse-grained, low-CEC aquifers to limit the freshwater loss by buoyancy effects (van Ginkel, 2015). The retarded arrival during salinization at the deepest recovering well can also positively affect the RE when slightly elevated Na^+ concentrations are acceptable.

Reactive transport modelling highlighted that a central layer with a high CEC can cause Na^+ contamination of a significant freshwater volume. For the Nootdorp pilot however, the assumption of a relatively low CEC in the whole target aquifer best reproduced field observations, despite the presence of a unit with reworked clay and peat fragments for which a high CEC was determined. Possibly, this contradiction is due to the discontinuous nature of this unit (GU-III) and/or by the fact that the clay and peat in this unit is concentrated in pebbles (see Supplementary Information), while most flow will occur in the less reactive surrounding sand matrix of this unit.

Although dosing of Ca^{2+} to the injection water leads to a smaller water volume in which Na^+ is mobilized, the Na^+ concentration will increase proportionally. The water with mobilized Na^+ may still reach the top of the recovering wells and hamper later recovery. Addition of Ca^{2+} to the injection water will not lead to additional retardation of Na^+ when all Na^+ is already washed from the exchanger sites with the original injection water. A more positive

effect of Ca^{2+} dosing on the recovered water quality is expected with higher CECs and/or native salinities. Despite the deterioration by Na^+ desorption, an MPPW-equipped ASR system will still recover up to 3 times more water with low Na^+ concentrations compared to a fully penetrating well at the Nootdorp pilot (Zuurbier et al., 2014). However, a fully-penetrating ASR well in a brackish or saline aquifer may outperform the MPPW when already a small increase of Na^+ concentrations is unacceptable and/or when a much larger part of the injected water is forced through high-CEC layers during MPPW-ASR.

4.2. Increasing Fe^{2+} and Mn^{2+} concentrations during MPPW-ASR

4.2.1. Mobilization during freshwater injection

Both mixing and cation exchange could not explain the observed (continuous) increase in Fe^{2+} and Mn^{2+} in the injected water (Section 3.3.1). Due to the high carbonate content and the potentially significant contribution of Fe and Mn to the carbonates (Fig. 3), dissolution of Fe and Mn-containing carbonates was suspected to be a source for mobilization. The amount of calcium mobilization in especially Cycle 1 could be only partly explained by equilibrium calcite dissolution enhanced by proton-buffering upon pyrite oxidation (Fig. 9). Particularly in Cycle 1, processes other than pyrite-oxidation stimulated calcite dissolution, such as oxidation of Fe^{2+} , Mn^{2+} , and SOM (see the reactions in Table 1). Based on the Ca^{2+} and HCO_3^- concentrations observed, oxygen was partly consumed by the oxidation of Fe^{2+} and Mn^{2+} rather than SOM (Fig. 9). With the observed Ca^{2+} and DO concentrations in the injection water and the dissolution processes, the resulting Ca^{2+} and SO_4^{2-} concentrations could be explained.

Since the observed Ca^{2+} concentrations can be explained by equilibrium dissolution and acid buffering upon proton and CO_2 -production, it is concluded that the dissolved carbonate was merely pure calcite. The lasting enrichment of Fe^{2+} and Mn^{2+} in the deeper aquifer interval (constantly $\sim 3 \mu\text{mol/l}$ in Cycle 2) indicates that less than 1% of the dissolved carbonate was in the form of Fe and Mn-carbonates. This was sufficient to create an undesirable Fe^{2+} and especially Mn^{2+} enriched water type.

In the upper aquifer interval (GU-I, level S2), other processes

than pyrite oxidation in both cycles prevailed, which was presumably caused by the lower pyrite and higher SOM content (Table 3). Based on the low Ca^{2+} and SO_4^{2-} production and the geochemical composition, oxidation of organic matter was the most likely lasting process of oxygen consumption. Mobilization of Fe^{2+} and Mn^{2+} was limited for this reason and due to the purer calcite (Fig. 3) and the absence of periodic salinization.

4.2.2. Mobilization of Mn^{2+} during recovery

Fe^{2+} and Mn^{2+} concentrations of $\sim 3 \mu\text{mol/l}$ were mobilized in the deeper aquifer but not encountered during recovery. Instead, the recovered water had a much higher Mn:Fe ratio in comparison with the water at MW1. A general shift occurred from a Fe^{2+} -dominated water type to a Mn^{2+} -dominated water type. This suggests that especially Fe-hydroxides precipitated, which potentially increased the sorption of especially Fe^{2+} . Mn-oxides (like MnO_2) may also have formed close to injecting ASR wells by oxidation of (adsorbed) Mn^{2+} during injection phases. However, they were likely reduced by Fe^{2+} by anoxic water during recovery phases, causing the increase of the Mn:Fe ratio. This process (Table 1), which is described by Postma and Appelo (2000), is relatively fast (Postma, 1985). Part of the Fe^{2+} immobilization and Mn^{2+} enrichment could also have been caused by sorption of Fe^{2+} by $\text{Fe}(\text{OH})_3$, inducing proton-buffering via dissolution of Fe- and Mn-carbonates. However, Fe^{2+} concentrations observed at 5 m from the ASR-well were generally half the Mn^{2+} concentrations reaching the ASR well (Fig. 8). This suggests that MnO_2 reduction was the dominant process driving the mobilization, with 1 mol of Mn^{2+} produced through the oxidation of 2 mol of Fe^{2+} (Table 1).

4.2.3. Overall effect of MPPW-ASR on Fe^{2+} and Mn^{2+} in the recovered water

At the Nootdorp site, the deep aquifer intervals of preferential injection coincide with an aquifer interval which is pyrite-rich and contains Fe and Mn-bearing carbonates. The Fe^{2+} and Mn^{2+} released upon dissolution could travel relatively unhampered towards the shallow AWS1, where no injection occurred and Fe-hydroxides and Mn-oxides to adsorb Fe^{2+} and Mn^{2+} were absent (Fig. 10). The positioning of the different reactive aquifer units is therefore unfavorable as the oxygen in the injected water is consumed by processes that negatively influence the water quality. Geochemically, injection would be preferred in the shallow GU-I, such that oxygen would be mainly consumed by organic matter in presence of a relatively pure calcite to buffer the associated increase in CO_2 pressure.

The Nootdorp MPPW-ASR pilot illustrates that the presence and the exact depth interval of reactive layers have a major impact on the recovered water quality. In contrast with conventional ASR in freshwater aquifers, the bulk recovered water quality is not controlled by the average geochemical composition of the target aquifer, but dominated by the reactivity of deeper aquifer segments where most injection occurs. During MPPW-ASR, a much larger part of the injected water had to pass the deeper (sub)horizontal reactive units. The (sub)horizontal geochemical stratification of sedimentary aquifers therefore deserves more attention.

4.2.4. Dealing with Mn^{2+} and Fe^{2+} mobilization

The recovery of Mn^{2+} and especially Fe^{2+} can be controlled by periodically injecting a small portion of the oxic injection water at the shallow recovery well. The system then injects a little more like a conventional ASR-well, creating precipitates around the recovering wells by oxidation of adsorbed and released Fe^{2+} and Mn^{2+} without significantly decreasing the aquifer permeability (Mettler et al., 2001). This process of subsurface iron removal (SIR) may be preferred over aboveground iron removal, as it does not create a

waste stream. Antoniou et al. (2014) pre-treated anoxic sediment columns from the GU-V with KMnO_4 , to create neo-formed Mn-oxides that increase the adsorption of Mn^{2+} and Fe^{2+} . This method has two main advantages: (1) MnO_4^- is a strong oxidant leading to extensive oxidation/depletion of pyrite, SOM, and Fe and Mn-carbonates, and (2) the oxidation reactions increase the pH which accelerates the precipitation of Mn-oxides and raises the sorption capacity for Fe^{2+} , Mn^{2+} , and As.

4.2.5. Behavior of arsenic at the Nootdorp MPPW-ASR pilot

As-mobilization decreased under more-and-more oxidized conditions around the ASR wells. Mn-oxides and Fe-hydroxides formed during injection likely facilitated As-adsorption. The passing of a clear and high As-peak early during injection suggest that a transition of As (III) to As(V) under oxidizing conditions was a boundary condition for As-adsorption, as observed in a similar target aquifer at approximately nearby (Stuyfzand, 1998; Wallis et al., 2010). Remobilization was not observed in the recovered freshwater. The observed As-release during salinization can be caused by anion exchange when the anions in the ambient groundwater (such as PO_4^{3-} and HCO_3^- (Stuyfzand et al., 2006)) pass and by reduction of the formed Fe-hydroxides (Lazareva et al., 2015). This may alter the native brackish water around the MPPW-ASR system in Nootdorp, rather than the injected freshwater.

5. Conclusions

Reactive transport processes resulted in increases in Na^+ , Fe^{2+} , Mn^{2+} , and As concentrations during the Nootdorp MPPW-ASR pilot. A significant freshwater volume was enriched with especially Na^+ due to cation exchange during freshening at the base of the target aquifer with every injection phase. Na^+ -enriched water was subsequently recovered by the shallow recovery wells due to the upward flow paths. As the arrival of Na^+ during salinization of the deeper aquifer interval was retarded by cation exchange, the net effect on the recovery efficiency (RE) during MPPW-ASR is site-specific and dependent on the CEC, the composition of the native groundwater and injected water, and the limits set for Na^+ in the recovered water. Unlike ASR systems in freshwater aquifers, negative effects from cation exchange on RE do not decrease cycle-after-cycle.

The release of Fe^{2+} and especially Mn^{2+} can caused deterioration of injected freshwater and was a consequence of mobilization by cation exchange during freshening, but primarily and lastingly by dissolution of Fe and Mn-bearing carbonates in the lower half of the target aquifer. Here, dissolution was promoted by proton-buffering and CO_2 production induced by pyrite oxidation (lasting) and the oxidation of primarily adsorbed Fe^{2+} and Mn^{2+} (mainly Cycle 1). The lack of injection at the shallowest recovery well prevented formation of Fe-hydroxides and Mn-oxides around this well and prevented adsorption of mobilized Fe^{2+} and Mn^{2+} prior to recovery. Since MnO_2 was an important oxidant for Fe^{2+} , mobilization of Mn^{2+} was the most prominent water quality threat. Precipitates to adsorb Mn^{2+} and Fe^{2+} close to the shallow recovery well(s) can be stimulated by periodic injections of small oxygen-rich water volumes ('subsurface iron removal'). Arsenic immobilized under oxidizing conditions and was remobilized during salinization.

More so than for ASR systems in freshwater aquifers, the interdependency of geochemical heterogeneity and the different aquifer intervals for deep injection, mobilization, and transport towards recovering wells is crucial for the resulting recovered water quality during MPPW-ASR. Detailed characterization of the vertical variation of geochemical properties is therefore preferred

to allow optimal placement of the MPPW well screens and development of a management strategy to combat potential water quality issues.

Acknowledgements

This research was funded by the Knowledge for Climate research program as part of its theme 'Climate Proof Freshwater Supply', the joint research program of the Dutch drinking water companies (BTO), and the EU FP7-projects DESSIN (grant agreement no. 619039) and SUBSOL (grant agreement no. 642228). The authors would like to thank Frans Backer, Michel Groen, John Visser, Martine Hagen, and Guido Beenakker for their assistance during fieldwork and lab analyses. Codema B-E De Lier and Van der Goes Orchideeën are thanked for their financial and practical support during installation and operation of the Nootdorp ASR-system. One anonymous reviewer, the associate editor, and Thomas Missimer are thanked for their comments on the earlier version of the manuscript.

Appendix A. Supplementary data

Supplementary data related to this article can be found at <http://dx.doi.org/10.1016/j.apgeochem.2016.05.013>.

References

- Antoniou, E.A., Hartog, N., van Breukelen, B.M., Stuyfzand, P.J., 2014. Aquifer pre-oxidation using permanganate to mitigate water quality deterioration during aquifer storage and recovery. *Appl. Geochem.* 50 (0), 25–36.
- Antoniou, E.A., van Breukelen, B.M., Putters, B., Stuyfzand, P.J., 2012. Hydro-geochemical patterns, processes and mass transfers during aquifer storage and recovery (ASR) in an anoxic sandy aquifer. *Appl. Geochem.* 27 (12), 2435–2452.
- Appelo, C.A.J., 1994a. Some calculations on multicomponent transport with cation exchange in aquifers. *Ground Water* 32 (6), 968–975.
- Appelo, C.A.J., 1994b. Cation and proton exchange, pH variations, and carbonate reactions in a freshening aquifer. *Water Resour. Res.* 30 (10), 2793–2805.
- Appelo, C.A.J., Postma, D., 2005. *Geochemistry, Groundwater and Pollution*, 2. A.A. Balkema, Leiden, The Netherlands, 649 pp.
- Breeuwsma, A., Wösten, J.H.M., Vleeshouwer, J.J., van Slobbe, A.M., Bouma, J., 1986. Derivation of land qualities to assess environmental problems from soil Surveys1. *Soil Sci. Soc. Am. J.* 50 (1), 186–190.
- Fortuin, N.P.M., Willemsen, A., 2005. Exsolution of nitrogen and argon by methanogenesis in Dutch ground water. *J. Hydrol.* 301 (1–4), 1–13.
- Hartog, N., Griffioen, J., van der Weijden, C.H., 2002. Distribution and reactivity of O₂-Reducing components in sediments from a layered aquifer. *Environ. Sci. Technol.* 36 (11), 2338–2344.
- Jones, G.W., Pichler, T., 2007. Relationship between pyrite stability and arsenic mobility during aquifer storage and recovery in southwest central Florida. *Environ. Sci. Technol.* 41 (3), 723–730.
- Kronzucker, H.J., Britto, D.T., 2011. Sodium transport in plants: a critical review. *New Phytol.* 189 (1), 54–81.
- Langevin, C.D., Thorne, D.T., Dausman, A.M., Sukop, M.C., Guo, W., 2007. SEAWAT version 4: a computer program for simulation of multi-species solute and heat transport. In: U.S.G.S. (Ed.), *Techniques and Methods*, Book 6, Reston, Virginia, USA.
- Lazareva, O., Druschel, G., Pichler, T., 2015. Understanding arsenic behavior in carbonate aquifers: implications for aquifer storage and recovery (ASR). *Appl. Geochem.* 52 (0), 57–66.
- Mettler, S., et al., 2001. Characterization of iron and manganese precipitates from an in situ ground water treatment plant. *Groundwater* 39 (6), 921–930.
- National Research Council, 1977. *Arsenic: Medical and Biological Effects of Environmental Pollutants*. The National Academies Press.
- Neil, C.W., Yang, Y.J., Schupp, D., Jun, Y.-S., 2014. Water chemistry impacts on arsenic mobilization from arsenopyrite dissolution and secondary mineral precipitation: implications for managed aquifer recharge. *Environ. Sci. Technol.* 48 (8), 4395–4405.
- Parkhurst, D.L., Appelo, C.A.J., 1999. User's Guide to PHREEQC (Version 2): a Computer Program for Speciation, Batch-reaction, One-dimensional Transport, and Inverse Geochemical Calculations. Water-resources Investigations Report; 99–4259. U.S. Geological Survey : Earth Science Information Center, Open-File Reports Section [distributor], Denver, Colorado, USA.
- Postma, D., 1985. Concentration of Mn and separation from Fe in sediments—I. Kinetics and stoichiometry of the reaction between birnessite and dissolved Fe(II) at 10°C. *Geochim. Cosmochim. Acta* 49 (4), 1023–1033.
- Postma, D., Appelo, C.A.J., 2000. Reduction of Mn-oxides by ferrous iron in a flow system: column experiment and reactive transport modeling. *Geochim. Cosmochim. Acta* 64 (7), 1237–1247.
- Price, R.E., Pichler, T., 2006. Abundance and mineralogical association of arsenic in the Suwannee Limestone (Florida): implications for arsenic release during water–rock interaction. *Chem. Geol.* 228 (1–3), 44–56.
- Pyne, R.D.G., 2005. *Aquifer Storage Recovery – a Guide to Groundwater Recharge through Wells*. ASR Systems LLC, Gainesville, Florida, USA, 608 pp.
- Russel, M. (Ed.), 2013. *Clogging Issues Associated with Managed Aquifer Recharge Methods*, 212 pp.
- Simcore Software, 2010. *Processing Modflow 8: an Integrated Modeling Environment for the Simulation of Groundwater Flow, Transport and Reactive Processes*.
- Stuyfzand, P.J., 1993. *Hydrochemistry and Hydrology of the Coastal Dune Area of the Western Netherlands*. Vrije Universiteit, Amsterdam, The Netherlands, 366 pp.
- Stuyfzand, P.J., 1994. Geohydrochemical aspects of methane in Dutch groundwater (in Dutch). *H2O* 27 (17), 500–510.
- Stuyfzand, P.J., 1998. Quality changes upon injection into anoxic aquifers in the Netherlands: evaluation of 11 experiments. In: Peter, J.H. (Ed.), *Artificial Recharge of Groundwater*, Proc. 3rd Intern. Symp. On Artificial Recharge. Balkema, Amsterdam, The Netherlands, pp. 283–291.
- Stuyfzand, P.J., 2008. Base exchange indices as indicators of salinization or freshening of (coastal) aquifers saltwater intrusion meeting. In: IFAS Research, Naples, Florida, USA, pp. 262–265.
- Stuyfzand, P.J., Van Rossum, P., Mendizabal, I., 2006. Does arsenic, in groundwater of the compound Rhine-Meuse-Scheldt-Ems delta, menace drinking water supply in The Netherlands? In: Appelo, C.A.J. (Ed.), *Arsenic in Groundwater, a World Problem*, Utrecht.
- Valocchi, A.J., Street, R.L., Roberts, P.V., 1981. Transport of ion-exchanging solutes in groundwater: chromatographic theory and field simulation. *Water Resour. Res.* 17 (5), 1517–1527.
- Van Beek, C.G.E.M., 1985. Experiences with underground water treatment in the Netherlands. *Water Supply* 3 (2), 1–11.
- van Ginkel, M., 2015. Aquifer design for freshwater storage and recovery in artificial islands and coastal expansions. *Hydrogeol. J.* 23 (4), 615–618.
- van Halem, D., Vet, W.d., Verberk, J., Amy, G., van Dijk, H., 2011. Characterization of accumulated precipitates during subsurface iron removal. *Appl. Geochem.* 26 (1), 116–124.
- Van Helvoort, P.J., 2003. *Complex Confining Layers: a Physical and Geochemical Characterization of Heterogeneous Unconsolidated Fluvial Deposits Using a Facies-based Approach*. Utrecht University, Utrecht.
- Vanderzalm, J.L., et al., 2011. Arsenic mobility and impact on recovered water quality during aquifer storage and recovery using reclaimed water in a carbonate aquifer. *Appl. Geochem.* 26 (12), 1946–1955.
- Wallis, I., et al., 2011. Process-based reactive transport model to quantify arsenic mobility during aquifer storage and recovery of potable water. *Environ. Sci. Technol.* 45 (16), 6924–6931.
- Wallis, I., Prommer, H., Post, V., Vandenbohede, A., Simmons, C.T., 2013. Simulating MODFLOW-based reactive transport under radially symmetric flow conditions. *Groundwater* 51 (3), 398–413.
- Wallis, I., Prommer, H., Simmons, C.T., Post, V., Stuyfzand, P.J., 2010. Evaluation of conceptual and numerical models for arsenic mobilization and attenuation during managed aquifer recharge. *Environ. Sci. Technol.* 44 (13), 5035–5041.
- Ward, J.D., Simmons, C.T., Dillon, P.J., Pavelic, P., 2009. Integrated assessment of lateral flow, density effects and dispersion in aquifer storage and recovery. *J. Hydrol.* 370 (1–4), 83–99.
- Weltje, G.J., Tjallingii, R., 2008. Calibration of XRF core scanners for quantitative geochemical logging of sediment cores: theory and application. *Earth Planet. Sci. Lett.* 274 (3–4), 423–438.
- Zuurbier, K., Bakker, M., Zaadnoordijk, W., Stuyfzand, P., 2013. Identification of potential sites for aquifer storage and recovery (ASR) in coastal areas using ASR performance estimation methods. *Hydrogeol. J.* 21 (6), 1373–1383.
- Zuurbier, K.G., Zaadnoordijk, W.J., Stuyfzand, P.J., 2014. How multiple partially penetrating wells improve the freshwater recovery of coastal aquifer storage and recovery (ASR) systems: a field and modeling study. *J. Hydrol.* 509 (0), 430–441.